



Published in final edited form as:

Cell Rep. 2018 April 03; 23(1): 112–126. doi:10.1016/j.celrep.2018.03.039.

Identification of CDC25 as a Common Therapeutic Target for Triple-Negative Breast Cancer

Jeff C. Liu¹, Letizia Granieri^{1,2,13}, Mariusz Shrestha^{1,3,13}, Dong-Yu Wang¹, Ioulia Vorobieva^{1,3}, Elizabeth A. Rubie⁴, Rob Jones¹, YoungJun Ju¹, Giovanna Pellecchia^{5,6}, Zhe Jiang¹, Carlo A. Palmerini², Yaacov Ben-David^{8,9}, Sean E. Egan^{10,11}, James R. Woodgett⁴, Gary D. Bader^{5,10}, Alessandro Datti^{2,7}, Eldad Zacksenhaus^{1,3,12,14,*}

¹Toronto General Research Institute - University Health Network, 67 College Street, Toronto, ON, Canada M5G 2M1

²Department of Agriculture, Food, and Environmental Sciences, University of Perugia, Perugia, Italy

³Department of Laboratory Medicine & Pathobiology, University of Toronto, Toronto, ON, Canada

⁴Lunenfeld-Tanenbaum Research Institute, Sinai Health System, 600 University Avenue, Toronto, ON, Canada

⁵The Donnelly Centre, University of Toronto, Toronto, ON, Canada

⁶The Centre for Applied Genomics, The Hospital for Sick Children, Toronto, ON, Canada

⁷Network Biology Collaborative Centre, SMART Laboratory for High-Throughput Screening Programs, Mount Sinai Hospital, Toronto, ON, Canada

⁸The Key Laboratory of Chemistry for Natural Products of Guizhou Province and Chinese Academic of Sciences, Guiyang, Guizhou 550014, China

⁹State Key Laboratory for Functions and Applications of Medicinal Plants, Guizhou Medical University, Guiyang, Guizhou 550025, China

¹⁰Department of Molecular Genetics, University of Toronto, Toronto, ON, Canada

¹¹Program in Cell Biology, The Peter Gilgan Center for Research and Learning, The Hospital for Sick Children, Toronto, ON, Canada

This is an open access article under the CC BY-NC-ND license (<http://creativecommons.org/licenses/by-nc-nd/4.0/>).

*Correspondence: eldad.zacksenhaus@utoronto.ca.

AUTHOR CONTRIBUTIONS

Conceptualization, J.C.L. and E.Z.; Experimentations, J.C.L., L.G., M.S., I.V., R.J., E.A.R., Y.J., and Z.J.; Bioinformatics Analysis, J.C.L., D.-Y.W., and G.P.; Supervision, J.R.W., G.D.B., C.A.P., A.D., and E.Z.; Funding Acquisition, J.R.W., S.E.E., C.A.P., G.D.B., A.D., and E.Z.; Writing – Original Draft, J.C.L., J.R.W., and E.Z.; Writing – Review & Editing, J.R.W., M.S., I.V., J.Z., S.E.E., Y.B.-D., G.D.B., A.D., and E.Z. All authors reviewed and edited the final manuscript.

Additional experimental procedures can be found in the Supplemental Information.

SUPPLEMENTAL INFORMATION

Supplemental Information includes Supplemental Experimental Procedures and eight figures and can be found with this article online at <https://doi.org/10.1016/j.celrep.2018.03.039>.

DECLARATION OF INTERESTS

The authors declare no competing interests.

¹²Department of Medicine, University of Toronto, Toronto, ON, Canada

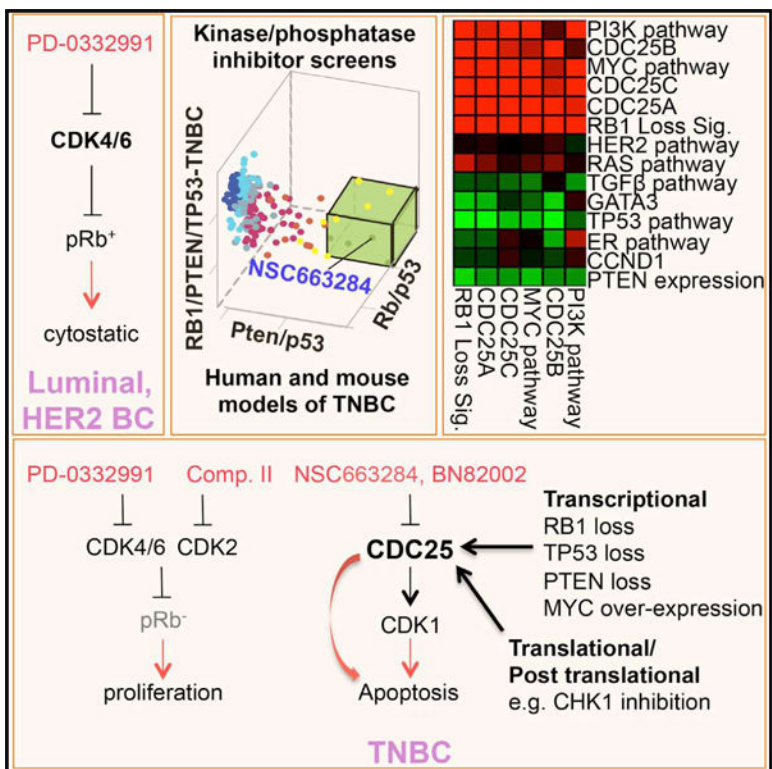
¹³These authors contributed equally

¹⁴Lead Contact

SUMMARY

CDK4/6 inhibitors are effective against cancer cells expressing the tumor suppressor RB1, but not RB1-deficient cells, posing the challenge of how to target RB1 loss. In triple-negative breast cancer (TNBC), *RB1* and *PTEN* are frequently inactivated together with *TP53*. We performed kinome/phosphatase inhibitor screens on primary mouse *Rb/p53*-, *Pten/p53*-, and human *RB1/PTEN/TP53*-deficient TNBC cell lines and identified CDC25 phosphatase as a common target. Pharmacological or genetic inhibition of CDC25 suppressed growth of RB1-deficient TNBC cells that are resistant to combined CDK4/6 plus CDK2 inhibition. Minimal cooperation was observed *in vitro* between CDC25 antagonists and CDK1, CDK2, or CDK4/6 inhibitors, but strong synergy with WEE1 inhibition was apparent. In accordance with increased PI3K signaling following long-term CDC25 inhibition, CDC25 and PI3K inhibitors effectively synergized to suppress TNBC growth both *in vitro* and in xenotransplantation models. These results provide a rationale for the development of CDC25-based therapies for diverse *RB1/PTEN/TP53*-deficient and -proficient TNBCs.

Graphical Abstract



In Brief

Liu et al. report that inhibition of the protein phosphatase CDC25 kills diverse triple-negative breast cancer (TNBC) cells. Moreover, CDC25 antagonists cooperate with other drugs, such as PI3K inhibitors, to efficiently suppress growth of human TNBC engrafted into mice.

INTRODUCTION

Breast cancer (BC), a leading cause of death from malignancies in women worldwide, comprises three major pathological subtypes: ER⁺, HER2/NEU/ERBB2⁺, and triple-negative BC (TNBC) (Curtis et al., 2012; Koboldt et al., 2012; Nik-Zainal et al., 2016; Prat and Perou, 2011). TNBCs include basal-like and claudin-low tumors that are highly aggressive. TNBCs are treated with chemotherapy/radiation; no targeted therapy is currently available. The tumor suppressor genes *RB1* and *PTEN* are frequently lost together with *TP53* in TNBC. Using different bioinformatics approaches, *RB1* and *TP53* were estimated to be lost together in 28% of TNBC, and *PTEN* plus *TP53* in ~19% (Jones et al., 2016) (Liu et al., 2014). RB1 exerts its anti-proliferative effects by binding to and inhibiting the function of activating E2F1–3 transcription factors, which regulate the expression of genes required for cell-cycle progression (Kitajima and Takahashi, 2017; Liu et al., 2015; Zacksenhaus et al., 2017). G1 cyclin-dependent kinase CDK4/6-cyclin D and CDK2-cyclin E complexes phosphorylate and inactivate pRb, leading to cell-cycle progression. In BC and other malignancies in which *RB1* is intact, pRb is invariably inactivated through hyper-phosphorylation in response to amplification or overexpression of CYCLIN Ds, CYCLIN Es, CDK4/6, or CDK2 or loss of negative regulators such as the CDK4/6 inhibitor p16^{INK4A}. Thus, BCs that are ER⁺ or HER2⁺ and express hyper-phosphorylated pRb are highly sensitive to cytostatic effects of CDK4/6 inhibitors such as PD0332991 *in vitro* (Finn et al., 2009). Indeed, these drugs have shown great promise in clinical trials (reviewed in Knudsen and Witkiewicz, 2017; Otto and Sicinski, 2017). BC cells that do not express RB1 respond poorly to PD0332991. In addition, recurrent disease is often accompanied by RB1 loss (Herrera-Abreu et al., 2016). RB1 deficiency is not druggable (Jiang et al., 2011); moreover, as shown herein, combined treatments with CDK4/6 plus CDK2 inhibitors weakly suppress growth of RB1-deficient TNBC cells compared to RB1-proficient cells. Loss of the tumor suppressor PTEN in TNBC also poses a clinical challenge. PTEN is a phosphatase that antagonizes phosphatidylinositol 3-kinase (PI3K) signaling by dephosphorylating phosphatidylinositol 3,4,5-trisphosphate (PIP₃) (Wang et al., 2017, and references therein). PTEN-deficient TNBCs respond to PI3K inhibitors; however, PI3K inhibition often leads to relapse and even promotes tumor dissemination by inducing mitochondrial activity (Caino et al., 2015), suggesting that combination therapy is needed for effective treatment. Finally, the RB1 pathway (RB1; p16^{INK4A}), PI3K pathway (PIK3CA; PTEN), and TP53 are major drivers of metastasis in diverse cancer types (Robinson et al., 2017). There is, therefore, an urgent need to identify therapeutic targets for TNBC and other malignancies with alterations in these pathways.

To dissect the genetic behavior of these tumors and identify potential targets, we generated mouse models for *Rb/p53*- and *Pten/p53*-deficient TNBC (Jiang et al., 2010; Jones et al., 2016; Liu et al., 2014; Wang et al., 2016). In each case, we identified downstream vulnerabilities that can be exploited therapeutically. Specifically, for *PTEN/TP53* loss, we

identified eEF2K as a therapeutic target downstream of PI3K-mTOR signaling (Liu et al., 2014); for *RB1/TP53* deficiency, we identified the mitochondrial protein translation pathway downstream of RB1-E2F1/3 (Jones et al., 2016). To search for pathways/inhibitors that can target aggressive TNBCs with alterations in these pathways, we herein performed kinase/phosphatase screens on primary mouse *Rb/p53*- and *Pten/p53*-deficient tumor cells as well as human TNBC lines with mutations in these genes. We describe the identification of the dual-specificity protein phosphatase CDC25 (cell division cycle 25) as a key target for these divergent TNBC types both *in vitro* and in xenograft assays. CDC25 removes inhibitory phosphate residues from various cyclin-dependent kinases (CDKs) including CDK1, the only essential CDK in mammals (Santamaría et al., 2007). There are three variants of CDC25, CDC25A–C, that play critical roles in DNA-damage responses and the G1/S and G2/M transitions (Boutros et al., 2007). Although CDC25 inhibitors were previously investigated as potential therapies for various cancers, including BC (Cangi et al., 2000), the pathophysiological context in which these drugs may be effective has not been defined. Our results suggest that, while CDK4/6 antagonists are effective against RB1⁺, ERα⁺ luminal, or HER2⁺ BCs, inhibitors of CDC25, alone or in combination with other components of the CDC25 pathway such as WEE1, offer potent interventions to treat aggressive RB1⁻, PTEN⁻, and TP53-deficient TNBCs.

RESULTS

Weak Effect of CDK4/6 Plus CDK2 Inhibitors on RB1-Deficient TNBC Cells

TNBCs are refractory to the CDK4/6 inhibitor PD0332991 (Finn et al., 2009; Robinson et al., 2013). As these tumors often exhibit high levels of cyclin E, we asked whether the presence or absence of RB1 modulated TNBC sensitivity to the CDK2 Inhibitor II (EMD Millipore) (Davis et al., 2002), either alone or in combination with PD0332991. Growth inhibition by 3-(4,5-dimethylthiazol-2-yl)-2,5-diphenyltetrazolium bromide (MTT) assay was determined 3 days post-treatment with low doses of each drug. Synergy was assessed by CompuSyn analysis (<http://www.combosyn.com>) (Chou and Talalay, 1984), in which a combination index (CI) < 0.85 denotes synergy, a CI of 0.9–1.0 denotes additive effects, and a CI > 1.1 denotes antagonistic effects. The RB1 status in these TNBC lines is indicated: BT549 and MDA-MB-436 harbor both RB1 and PTEN alterations, and all lines contain TP53 mutations/deletions. With the exception of HCC38, the RB1⁺ tumor lines exhibited greater sensitivity to CDK4/6 plus CDK2 inhibitors than lines deficient in RB1. Moreover, we found strong and moderate synergy between PD0332991 and the CDK2 inhibitor in the RB1⁺ lines MDA-MB-231 and MDA-MB-157, respectively, but no effect in RB1⁺ HCC38 TNBC cells and none in all three RB1-deficient TNBC lines (BT549, MDA-MB-436, and MDA-MB-468; Figure S1A). Flow cytometry analysis using annexin V/PI staining corroborated these results, showing increased apoptosis in the RB1-positive MDA-MB-231 but not in RB1-deficient BT549 cells following combined treatment with the CDK4/6 and CDK2 inhibitors (Figure S1B). To identify a possible common target for TNBC, we interrogated these human TNBC lines along with primary cultures from *Rb/p53*- and *Pten/p53*-deficient mouse mammary tumors, as described below.

Common and Distinct Features of *Rb/p53*- and *Pten/p53*-Deficient Mammary Tumors

To gauge the gene expression differences and similarities between *Rb/p53* and *Pten/p53* mammary tumors, we first performed unsupervised hierarchical clustering with mouse and human BC samples (Herschkowitz et al., 2007; Liu et al., 2014). Batch correction and integration were performed via “distance weighted discrimination” (DWD), using normal mouse mammary glands and tumors from MMTV-*Her2/Neu* mice as internal controls. With three exceptions, all *Rb/p53* and *Pten/p53* mammary tumors clustered with other mouse models of spindle-shape tumors, which closely resemble human claudin-low (CL) and basal-like BC (Figure 1A). Outliers included two *Pten/p53* tumors that clustered with mouse *Pten* tumors and one *Rb/p53* tumor that clustered with basal-like SV40 large Tag tumors.

We next used a claudin-low signature developed by Prat and Perou (Prat et al., 2010). Again, with the exception of the same three outliers, *Rb/p53* and *Pten/p53* mammary tumors clustered together with human claudin-low BC (Figure 1B). In these analyses, the *Rb/p53* and *Pten/p53* mammary tumors clustered near each other but as two distinct groups, suggesting some differences but otherwise much similarity between these tumor types. We then performed pathway analysis using gene set enrichment analysis (GSEA) on the claudin-low-like *Rb/p53* and *Pten/p53* tumors and visualized results as an enrichment map generated through Cytoscape software at high stringency ($p < 0.005$, and false discovery rate [FDR] $Q < 0.05$). Multiple pathways were elevated in *Rb/p53* versus *Pten/Rb* tumors, including cell stemness such as WNT, fetal/embryonic development, and heart development (Figure 1C; Figure S2A). Expression of proliferation, epithelial-mesenchymal transition (EMT), and hypoxia genes was induced in both *Rb/p53* and *Pten/p53* tumors compared with other subtypes (Figure S2B). As a prelude to the analysis discussed later, we specifically examined the expression of genes on the *Cdc25* pathway. Expression of *Cdc25* pathway genes—and, specifically *Cdc25B* and *Cdc25C*—was induced in *Rb/p53*-, *Pten/p53*-, and *p53*-deficient tumors relative to *Pten* loss and normal mammary gland, respectively (Figure 1D; statistical analysis is given in Figure S3).

Focused Drug Screens of Mouse *Rb/p53*- and *Pten/p53*-Deficient Mammary Tumors and Human *RB1/PTEN/TP53* Mutant BC Lines Identify *CDC25* as a Common Target

While *RB1* loss disrupts G1/S checkpoint control, other checkpoints may still be functional and critical regulators of growth for *RB1*-deficient TNBC. To identify such Achilles' heels, we performed a focused screen of 238 compounds targeting 154 different protein kinases and phosphatases (3 μM) for multiple cell-cycle transitions. We screened two primary cultures from *Rb/p53*-deficient tumors; four primary *Pten/p53*-deficient tumors; and two human TNBC lines; BT549 and MDA-MB-436, both with mutations/deletions in all three tumor suppressor genes (*RB1*, *PTEN*, and *TP53*). We set a cutoff of 2-fold growth suppression by alamar blue staining 3 days post-drug treatment (single dose). A *CDC25* inhibitor, NSC663284, exerted the strongest and most consistent growth inhibition on all three groups of tumor cells (Figures 2A–2C). Three other compounds were identified: staurosporine, a pan-kinase inhibitor; IKK16, a selective inhibitor of $\text{I}\kappa\text{B}$ kinases *IKK α* and *IKK β* ; and FAK inhibitor 14, a non-specific FAK inhibitor. *CDC25* inhibition has been previously shown to suppress growth of diverged cancer types, including BC (Boutros et al., 2007; Kristjánssdóttir and Rudolph, 2004). Our results suggest that this phosphatase, which

activates multiple CDKs, including cyclin-dependent kinase 1 (CDK1, human CDC2), may be particularly effective against TNBCs, which are resistant to CDK4/6 plus CDK2 inhibition.

Checkpoint kinases 1 and 2 (CHK1/2) are negative regulators of CDC25, which, in response to DNA damage, are induced to arrest cells at different stages of the cell cycle, thereby facilitating DNA repair (Bartek and Lukas, 2003; Medema and Macrek, 2012). Despite this tumor-suppressing function, CHK1 and CHK2 are elevated in cancer and act as oncogenes, so that their inhibition is therapeutic (Ma et al., 2011). Several CHK1 inhibitors, PD-407824, SB-218078, and TCS-2312, and one CHK2 inhibitor, NSC-109555, were identified in our screens but, with the exception of TCS-2312, were less potent than the CDC25 inhibitor (Figures 2B and 2D). TCS-2312 exhibited stronger inhibition than the CDC25 inhibitor on the two human TNBC lines but had weak effects on mouse *Rb/p53* and *Pten/p53* tumors (Figure 2D, light blue). Multiple inhibitors of the PI3K pathways were also found to suppress growth of *Pten/p53*-deficient mouse and human TNBCs by greater than 2-fold (Figure 2C, highlighted in red). These drugs also inhibited the growth of *Rb/p53*-deficient TNBC-like mammary tumor cells, although only the dual-PI3K/mTOR inhibitor NVB-BEZ235 suppressed growth over the 2-fold mark.

CDC25 Inhibition Diminishes Growth and Survival of RB1-Deficient and -Proficient TNBC Cells

Though highly potent *in vitro*, the quinolinedione CDC25 phosphatase inhibitor NSC663284 interacts with serum glutathione, and its activity is rapidly lost *in vivo* (Guo et al., 2007). Thus, to validate the inhibitory effect of CDC25 antagonists, we also examined the response of RB1-deficient TNBC cells to another CDC25 inhibitor, BN82002, which has a higher half maximal inhibitory concentration (IC₅₀) but better pharmacokinetics (Brezak et al., 2004) (Figure 2C). CDC25 dephosphorylates multiple substrates, including CDK1 on tyrosine-15 (Y15) (Boutros et al., 2007). To confirm the effect of these inhibitors on CDC25 in TNBC cells, NSC663284- or BN82002-treated cells were analyzed by immunoblotting with phospho-specific antibody for CDK1^{Y15}. These treatments increased Y15 phosphorylation in TNBC lines, confirming their antagonistic effects on CDC25 phosphatase activity in this cancer subtype (Figure 3A).

The three TNBC lines, MDA-MB-436, BT549, and MDA-MB-468, which were resistant to combined CDK4/6 plus CDK2 inhibitors (Figure S1), showed high and significant sensitivity to BN82002 (Figure 3B). Furthermore, multiple basal-like (basal A) and claudin-low (basal B) BC cells exhibited a lower IC₅₀ for BN82002 ($\leq 8.7 \mu\text{M}$) compared with luminal BC lines (CAMA1, MDA-MB-361, and MCF7; $>12 \mu\text{M}$; $p < 0.00324$; Figure 3C). To determine whether growth inhibition was cytostatic or cytotoxic, treated cells were subjected to annexin V/propidium iodide (PI) staining. All lines showed significant loss of viability upon BN82002 treatment (Figure 3D, bottom left quadrant). In MDA-MB-468 cells, growth inhibition was accompanied by apoptosis as defined by an increased annexin V/PI population (89.4%) relative to untreated cells (7.7%). In contrast, MDA-MB-436 and BT549 cells exhibited an increase in the PI-positive necrotic tumor population, not annexin V-positive cells. Anti-CDC25 treatment of BT549 and MDA-MB-231 cells also induced

cleavage of PARP, a marker for caspase-dependent apoptosis (Figure 3E). Thus, CDC25 inhibition led to cytotoxic, not cytostatic, effect in all TNBC lines tested.

We next examined the effect of RB1 status on the response to BN82002 in isogenic MDA-MB-231 cells in which endogenous *RB1* was transiently knocked down via RNAi (Figure 3F). MDA-MB-231 cells treated with *RB1* RNAi or control scrambled RNA were then exposed to various doses of BN82002, and effect on growth was assessed by MTT assay. The control and *RB1* knocked-out MDA-MB-231 cells exhibited similar dose responses (Figure 3F), thus demonstrating that CDC25 inhibition is effective in both RB1-proficient and -deficient TNBCs.

***CDC25A* and *CDC25B* Expression Correlates with TNBC-Related Oncogenic Signaling, and Poor Clinical Outcome**

Although expression of CDC25 enzymes in BC has been investigated (Santamaría et al., 2007), the effect of specific oncogenic alterations on their expression and the impact on clinical outcome are not defined. Here, we correlated *CDC25* gene expression with *RB1*, *PTEN*, and *TP53* status as well as the status of other oncogenic signaling calculated on the basis of microarray data from 1,302 BC samples (Dvinge et al., 2013; Viré et al., 2014). An *RB1*-loss signature was based on the median expression values of 20 genes that are induced in response to *RB1* loss in different contexts (Herschkowitz et al., 2008). Probability activity for ER, HER2, MYC, TP53, PI3K, RAS, and transforming growth factor b (TGF-b) pathways was evaluated using mRNA expression data as defined by Gatz et al. (2010), and the status of *PTEN*, *GATA3*, and cyclin D1 was inferred from their expression.

CDC25 mRNA levels positively correlated with increased activity of the *RB1*-loss signature, loss of *TP53* activity signature, or reduced *PTEN* mRNA expression, the latter of which can be used as a surrogate for *PTEN* loss (Figure 4A) (Wang et al., 2017). *CDC25* expression also increased with elevated PI3K and MYC activity signatures, and slightly with RAS signaling, all major markers of TNBC. Conversely, *CDC25* expression diminished in tumors with high signatures or markers for HER2⁺ and ER⁺ subtypes (HER2 and ER signatures; *GATA3* and *CyclinD1* expression). These results are in accordance with established effects of TP53, RB/E2F, and *PTEN*, as well as MYC on *CDC25* gene expression (Dalvai et al., 2011; Vigo et al., 1999; Guo et al., 2013; Galaktionov et al., 1996).

To determine which BC subtypes exhibit increased *CDC25* expression in response to disruption of RB1, *PTEN*, and TP53, we classified the tumors and performed a correlation analysis on each subtype. ER signaling was used as a control for luminal tumors. Expression of *CDC25* genes most significantly correlated with RB1, TP53, and *PTEN* loss in TNBC (Figure 4B; for a statistical analysis, see Figure S4). We next determined the subtypes in which *CDC25* genes are highly expressed. Interestingly, expression of *CDC25A* and *CDC25B* was most elevated in basal-like BC, whereas highest *CDC25C* expression was detected in luminal B (Figure 4C).

We next tested for the impact of *CDC25* expression on disease-specific survival, available with this database of 1,302 BC samples. High expression of *CDC25A* and *CDC25B* ($p < 0.0001$) and *CDC25C* ($p = 0.0097$) correlated with poor clinical outcome (Figure 4D).

Expression of these genes did not impact survival within basal-like samples (data not shown), suggesting that they serve as surrogates for basal-like or luminal B subtypes, respectively, both of which show a poor prognosis. Alternatively, TNBCs that do not express *CDC25* to a high level may acquire other, equally potent, mechanisms to promote cell growth. Together, these results indicate that high *CDC25A* and *CDC25B* expression correlates with the loss of RB1, PTEN, and TP53 in basal-like BC; is elevated in this subtype; and identifies patients with poor survival.

Knockdown of *CDC25A* Plus *CDC25B* Mimics the Effects of *CDC25* Antagonists

As drugs often have off-target effects, we asked whether specific knockdown of *CDC25A* and *CDC25B* via RNAi recapitulated the effect of *CDC25* inhibitory drugs on cell growth and survival. By western blot analysis, we observed higher expression of *CDC25B* than *CDC25A* in BT549 cells, and a combined knockdown of both genes induced an accumulation of phospho-Y15 CDK1 (Figure 5A). As with BN82002, a nearly complete loss of cell viability was observed following RNAi-based targeting of both *CDC25s* (Figures 5B and 5C). Moreover, like BN82002, knockdown of *CDC25A* plus *CDC25B* induced, primarily, apoptosis (annexin V+) in MDA-MB-468 cells but substantial necrosis in BT549 cells (Figure 5D versus 3D). Thus, the effect of BN82002 is likely on target, and TNBC cells that are refractory to CDK4/6-plus-CDK2 combination therapy are specifically sensitive to *CDC25* inhibition.

Long-Term *CDC25* Inhibition Induces Phosphorylation of c-Jun

Inhibition of *CDC25*—and, thereby, pCDK1—leads to cell-cycle arrest in normal cells. However, as shown earlier, in TNBC cells, both pharmacological and genetic inhibition of *CDC25* led to massive cell death. *CDC25* was implicated either directly or indirectly in cell survival through several mechanisms, including dephosphorylation and suppression of Apoptosis Signal-regulating Kinase 1 (ASK1), also known as Mitogen-Activated Protein Kinase Kinase Kinase 5 (MAP3K5) (Cho et al., 2015; Zou et al., 2001). Activated ASK1, in turn, induces cell demise by inducing the phosphorylation of several targets, including SAPK, JNK, and JUN (Tibbles and Woodgett, 1999). In short-term (1-hr) assays, *CDC25* inhibition did not induce detectable phosphorylation of any of these downstream factors (data not shown). However, after 24-hr treatment, levels of Ser73-c-JUN were strongly elevated in un-stimulated cells as well as in cells exposed for a short period of time to the stress-inducing agents anisomycin, insulin growth factor (IGF)1, or tumor necrosis factor α (TNF- α) (Hazzalin et al., 1998; Liu et al., 2000) (Figure 5E; see Discussion).

Synergistic Effects of *CDC25* with *WEE1* Inhibitors, but Not with *CDK4/6*, *CDC2*, or *CDK1* Antagonists

We next sought to determine whether *CDC25* inhibition synergizes with other inhibitors of cell-cycle progression. Using MTT assays and annexin V/PI flow cytometry, no synergy was found between *CDC25* and *CDK4/6* inhibitors or between *CDC25* and *CDK2* inhibitors (Figures S5 and S6).

The *WEE1* kinase phosphorylates and inactivates *CDK1* on the same sites (Y15) where it is dephosphorylated by *CDC25* (Figure S7A), and *WEE1* inhibitors are currently assessed

in several clinical trials. Using RB1⁺ (MDA-MB-231) and RB1⁻ (BT549) TNBC cells, we consistently found a strong synergy between the two CDC25 inhibitors (BN82002 and NSC663284) and the WEE1 inhibitor MK-1775 (AZD1775) within the linear range of drug inhibition (Figures 6A–6C; Figures S7B–S7D). In contrast, the CDC25 antagonists showed either additive or antagonistic effects with the CDK1 inhibitor RO3306. These results suggest that CDC25 acts upstream of CDK1 but exerts its pro-apoptotic effect through a different pathway than WEE1. Consistent with this notion, CDC25 and WEE1 inhibitors had different effects on cell-cycle progression in TNBC cells: CDC25 inhibition had no overt effect, whereas WEE1 inhibition enriched for cells in S phase (Figures 6D and 6E).

CDC25 Inhibition Synergizes with PI3K to Suppress Growth of Multiple TNBC Lines *In Vitro* and Attenuate Xenograft Growth *In Vivo*

For CDC25-based precision medicine, it would be important to identify the US Food and Drug Administration (FDA)-approved drugs that can synergize with CDC25 inhibitors. Therefore, we investigated whether BN82002 would synergize with FDA-approved inhibitors of RB1 or PTEN deficiency. For RB1 loss, we used tigecycline, the antibiotic and inhibitor of mitochondrial protein translation, recently shown to preferentially kill RB1/TP53-deficient TNBC (Jones et al., 2016). While each of these drugs alone effectively suppressed TNBC growth, we observed synergy only in MDA-MB-436, an additive effect in MDA-MB-468, and an antagonistic effect in BT549 cells (Figure 6F; Figure S8). To assess the effect of these drugs *in vivo*, we engrafted MDA-MB-436 cells into the mammary glands of immune-compromised NSG mice. When tumors became palpable, mice were randomized and injected with vehicle alone, BN82002, tigecycline, or both drugs. BN82002 strongly inhibited the kinetic of growth and final size/weight of the MDA-MB-468 TNBC xenografts (Figures 6G–6I). In combination with tigecycline, it had a small yet further significant effect on tumor suppression.

As PTEN is often lost in TNBC, we also tested for synergy between BN82002 and PI3K inhibitors. This analysis was also motivated by our observation that long-term (24-hr) treatment with CDC25 inhibitors induced the expression of phospho-Ser473-PKB/AKT in MDA-MB-231 cells (Figure 7A), possibly the results of feedback regulation that prolongs survival. pSer473-PKB/AKT in the PTEN mutant BT548 was constitutively high (data not shown). Using the dual PI3K/mTOR inhibitor NVP-BEZ235 (Liu et al., 2009), we observed robust synergy with BN82002 in four BC lines, MDA-MB-231, MDA-MB-156, BT549, and MDA-MB-468, and an additive effect in MDA-MB-436 (Figure 7B). In a side-by-side comparison with two other PI3K inhibitors, BEZ235 exhibited the highest synergy with BN82002 (CI = 0.23), the pan PI3K p110 $\alpha/\beta/\delta/\gamma$ inhibitor BKM120 also synergized effectively (CI=0.52), whereas the p110 α PI3K-specific inhibitor BYL719 showed moderate synergy (CI = 0.75; Figure 7C). Importantly, BN82002 treatment alone exerted strong inhibition of BT549 xenograft growth in immune-compromised mice ($p = 0.0027$ versus control; Figure 7D). Inhibition was further increased in the combination arm with BEZ235 ($p < 0.0001$ versus control; $p = 0.002$ versus BN82002). Together, these results show that CDC25 blockade alone can suppress the progression of aggressive TNBCs *in vivo*, as well as synergize with other drugs to effectively inhibit xenograft growth.

DISCUSSION

The critical role played by RB1 in TNBC and metastatic BC has prompted worldwide efforts to identify mechanisms to target its loss, which is not directly druggable. Here, we used focused kinase/phosphatase screens to identify agents that can suppress divergent types of TNBC cells with specific loss of RB1/TP53, PTEN/P53, or all three tumor suppressors. We report on the identification of the dual-specificity protein phosphatase CDC25 as a potent target for subduing these diverse TNBCs. Thus, despite an insensitivity to G1 inhibitors, most TNBCs maintain intact CDC25 checkpoints and are vulnerable to CDC25 antagonists. An antagonist of CHK1, an upstream regulator of CDC25, was also identified in our screens as a potent inhibitor of human TNBC, though not mouse Rb/p53 and Pten/p53 tumors. In addition, an inhibitor of WEE1, which antagonizes CDC25 by phosphorylating Y15-CDK1, potently inhibited both RB1-negative and -positive TNBCs and further synergized with CDC25 inhibitors to kill tumor cells. The robust synergy between CDC25 and WEE1 inhibitors should prompt a search for additional combinations between CDC25 antagonists and upstream regulators like ATM and CHK1 or downstream targets such as Aurora and polo-like kinases, the latter of which have already been implicated in TNBC (Dominguez-Brauer et al., 2015). In particular, while this paper was under consideration, the Witkiewicz and Knudsen group has shown that CHK1 suppression is synthetically lethal with RB1 loss in TNBC cells (Witkiewicz et al., 2018). Whether inhibition of CDC25 plus CHK1 is as synergistic as CDC25 plus WEE1 is yet to be determined.

We show that *CDC25A* and *CDC25B* have an elevated expression in TNBC and are bad prognostic indicators for BC patients. This is, at least in part, because these phosphatases serve as surrogates for TNBCs, which have poor clinical outcomes. However, high expression or activity of these genes may also underlie high cell proliferation/survival of TNBC. We show that loss of TP53, RB1, and PTEN—as well as increased PI3K and MYC and, to a lesser degree, RAS signaling—correlate with high *CDC25* expression, which likely increases dependency on CDC25 and responsiveness to its inhibition. As noted, TP53, RB1/E2F, PTEN, and MYC are known regulators of *CDC25* expression. As these tumor suppressors/oncogenes are major drivers of TNBC, our observations further point to CDC25 as a major target for therapy for these aggressive tumors. These phosphatases are also regulated post-transcriptionally and post-translationally by various factors such as CHK1 and F-box proteins β -TrCP1 and β -TrCP2 (Busino et al., 2003), and they may respond to different cellular stresses such as hypoxia. Analysis of two recent databases with quantitative proteomic and absolute protein levels (Lawrence et al., 2015; Tyanova et al., 2016) shows an increase in CDC25C or CDC25B protein levels in TNBC versus luminal tumor cell lines. However, due to the small number of samples, the increase in CDC25C does not reach significance, whereas the increase in CDC25B in TNBC lines ($n = 8$) becomes significant only when one outlier from the luminal group ($n = 7$) is removed (data not shown). Additional analysis is required to correlate CDC25 levels and activities with tumor response to its inhibitors.

Clinical application of CDC25 inhibitors is challenged by difficulty in drugging these phosphatases and associated toxicity. Several additional CDC25 inhibitors have been described (Brezak et al., 2009; He et al., 2013), but no drug with clinical utility is currently

available. Our results should encourage renewed efforts to use approaches such as large-scale screens for allosteric inhibitors that indirectly target the catalytic domain. Moreover, our findings suggest that drugs that preferentially inhibit CDC25B, with moderate inhibition of CDC25A and no effect on CDC25C, may be effective yet less toxic.

A complementary approach would be to use low doses of CDC25 inhibitors in combination with other drugs, as used herein. We found no synergy between CDC25 and CDC4/6, CDK2, or CDK1 inhibitors. However, CDC4/6 inhibition has both cell-autonomous and non-cell-autonomous effects, the latter of which involve the promotion of anti-tumor immunity by suppressing the proliferation of regulatory T cells (Goel et al., 2017). Thus, despite the lack of cooperation between CDC25 and CDK4/6 inhibitors in cultured cells, it would be of interest to test the combined effect of these drugs in immune-competent models of TNBC.

Only one TNBC line (of 5) showed synergy with tigecycline. This is unfortunate, given a recent observation that tigecycline effectively cooperates with imatinib to inhibit chronic myeloid leukemia stem cells and diminish tumorigenesis (Kuntz et al., 2017). However, in solid tumors (such as BC), we found that the cytostatic effects of tigecycline antagonized other drugs, such as doxorubicin (Jones et al., 2016), and here, it antagonized or failed to synergize with BN82002 in most TNBC lines.

In contrast to the aforementioned combinations, we found a high degree of synergism between CDC25 and PI3K inhibitors, both *in vitro* and *in vivo*. As CDC25 inhibition induced phospho-Ser473-PKB/AKT, CDC25-plus-PI3K combination therapy may not be limited to TNBC with alterations in the PI3K/PTEN pathway. Indeed, we showed that CDC25 and PI3K inhibitors synergized to effectively kill diverse TNBCs with and without mutations along the PI3K/PTEN pathway. How AKT/PKB is induced following long-term treatment of TNBC cells with CDC25 inhibitors is yet to be established.

CDC25 suppression induced cell demise, which was not associated with cell-cycle arrest in any specific phase, suggesting that death occurs at multiple stages of the cell cycle. This is in contrast to the effect of WEE1 inhibition, which led to the accumulation of cells in the S phase at the expense of G1 and G2/M. Thus, while these factors have opposing effects on CDK phosphorylation they have additional and unique pro-survival targets. How does inhibition of CDC25 promote apoptosis in TNBC cells? CDC25 was shown to suppress the stress response kinase ASK1, which affects the phosphorylation of SAPK, JNK, and downstream c-JUN (Cho et al., 2015; Tibbles and Woodgett, 1999; Zou et al., 2001). We found that CDC25 inhibition induced Ser73-c-Jun phosphorylation 24 hr post-treatment. This late induction may be a direct effect of ASK1 but may also be caused by an indirect feedback mechanism that sustains survival in the face of pro-apoptotic signals induced by CDC25 inhibition. Detection of ASK1 and phosphorylated ASK1 is notoriously difficult. It would be important to assess the level/activity of this kinase; the effects of blocking ASK1, JNK, or c-JUN on survival of cells exposed to CDC25 inhibitors; and whether this pathway is linked to hypoxia or other stress responses in TNBC. Further analysis of this pathway may uncover biological markers for efficacy of anti-CDC25 therapy or venues to potentiate the effect of CDC25 inhibitors.

Although we focused our analysis on TNBC, CDC25 inhibition may prove effective against other types of malignancies in which *RB1* and/or *PTEN* plus *TP53* are frequently inactivated, including retinoblastoma, serous cervical cancer, and pancreatic and lung cancers, as well as against recurrent metastatic disease where these tumor suppressor genes are often lost. CDC25-dependent checkpoint transitions may be particularly effective in tumors in which the G1/S checkpoint has been compromised by RB1 loss. We also show that combined inhibition of CDC25 plus PI3K effectively suppressed growth of TNBC cells in culture and in xenograft assays *in vivo*. We envision that improved CDC25 inhibitors would also be highly efficacious in combination therapy regimens together with inhibitors against specific oncogenic alterations in each individual TNBC patient, similar to the emerging clinical utility of CDK4/6 inhibitors in combination with endocrine or anti-HER2 therapies for RB1⁺ BC.

EXPERIMENTAL PROCEDURES

Mice

Animal protocols were approved by the University Health Network in accordance with the guidelines of the Canadian Council on Animal Care.

Tumor Classification

Microarray analysis with mouse tumor models was carried out using the Affymetrix Mouse Gene 1.0 ST with 500 ng total RNA isolated by double TRIzol extractions (Centre for Applied Genomics, Hospital for Sick Children, Toronto, ON, Canada). Microarray data were normalized using the robust multi-array average (RMA) method via Partek software, and log₂-transformed gene expression values were obtained. Median-centered data from aforementioned mouse models were integrated with a reference BC dataset (GEO: GSE18229), which includes both human and mouse subtypes, including human normal, luminal A, luminal B, HER2, claudin-low, and basal-like tumors, using the DWD algorithm. Unsupervised hierarchical clustering (complete linkage) analysis of mouse tumor models was determined using the intrinsic genes (Herschkowitz et al., 2007) and the claudin-low signature (Prat et al., 2010). For side-by-side comparison of mouse models, several groups of genes (Proliferation, EMT, and Hypoxia) were median centered and visualized as heatmaps.

Focused Drug Screens

238 compounds targeting 154 different kinases and phosphatases were screened using a Biomek FX liquid handler equipped with a pin tool for automated compound dispensing. Assays were carried out in a 384-well format, using 300 cells per well. Compounds, resuspended in DMSO as 1-mM stock solutions, were added in a volume of 200 nL to a final concentration of 3 μM. As a reference for 100% activity, each plate included 32 wells with cells treated with vehicle only, and background was measured with media in the absence of cells. Assays were optimized for dynamic range (100% activity per background, >10), while variability was consistently found to be low (i.e., coefficient of variation [CV] < 10%). For IC₅₀, cells were plated, at a concentration of 500 cells per well in 100 μL media, into 96-well plates and treated the next day with indicated compounds at increasing

concentrations (1, 3, 10, 30, and 100 μ M) for 3 days. Cell viability was measured by adding MTT to a final concentration of 1 mg/mL for 2 hr at 37°C, followed by a PBS wash and re-suspension in 100 μ L DMSO overnight. Colorimetric reading at 570 nm was performed using a microplate reader (Molecular Devices). Specific drugs for validation/analysis were as follows: BN82002 (EMD Millipore, catalog #21691), NSC663284 (ApexBio, catalog #A8813), RO3306 (ApexBio, catalog #A8885), and MK-1775 (ApexBio, catalog #A5755).

Gene Expression, Signature and Pathway Activity, and Statistical Analysis

Gene expression of CDC25A, CDC25B, and CDC25C, as well CCND1, GATA3 and PTEN, were represented as the median center expression values of the mRNA microarray data from 1,302 BCs (Dvinge et al., 2013; Viré et al., 2014) that were downloaded from the European Genome-phenome Archive (European Genome-phenome Archive: EGAS00000000122 and EGAD00010000434 at <https://www.ebi.ac.uk/ega/datasets/EGAD00010000434>). RB1-loss signature was based on the median expression values of 20 RB1-loss genes (Herschkowitz et al., 2008; Jones et al., 2016). Probability activity of the ER, HER2, MYC, P53, PI3K, RAS, and TGF- β pathways was evaluated using the microarray data as described previously (Gatza et al., 2010). With Prism 6 Software (GraphPad Software, La Jolla, CA, USA), Pearson correlation was used to evaluate the associations between the expression of the CDC25 gene family and oncogene/tumor suppressor activities that were represented as pathway-activity/signature/gene-expression values of mRNA expression of transcripts and compared with each other. An ANOVA was used to determine statistical significance of CDC25 family expression among the different subtypes of the human BCs. A log-rank (Mantel-Cox) test was performed for Kaplan-Meier plots. A p value < 0.05 was considered as statistically significant.

Xenograft Model

Human MDA-MB-436 and BT549 (1 million cells per injection) tumor cells were resuspended in 20 μ L media/Matrigel mixture (1:1) and injected into #4 mammary glands of non-obese diabetic/severe combined immunodeficiency (NOD/SCID) females (6 mice per group). BN82002 (15 mg/kg, dissolved in DMSO), tigecycline (50 mg/kg, dissolved in PBS), and BEZ235, as indicated, were administered intraperitoneally (i.p.). Control mice were injected with vehicle alone at the same weight/volume ratio.

Supplementary Material

Refer to Web version on PubMed Central for supplementary material.

ACKNOWLEDGMENTS

We thank Emily Reddy, from the SickKids-UHN Flow Cytometry Facility, for assistance with cell-cycle analysis. This research was funded by grants from the Canadian Cancer Society and the Canadian Institute of Health Research to E.Z.; by a Terry Fox Research Institute Program grant to J.R.W., S.E.E., and E.Z.; by the Government of Canada through Genome Canada and the Ontario Genomics Institute (OGI-088 and OGI-097) to A.D.; and by NIH grants P41 GM103504, U41 HG006623, and R01 GM070743 to G.D.B.

REFERENCES

- Bartek J, and Lukas J (2003). Chk1 and Chk2 kinases in checkpoint control and cancer. *Cancer Cell* 3, 421–429. [PubMed: 12781359]
- Boutros R, Lobjois V, and Ducommun B (2007). CDC25 phosphatases in cancer cells: key players? Good targets? *Nat. Rev. Cancer* 7, 495–507. [PubMed: 17568790]
- Brezak MC, Quaranta M, Mondésert O, Galcera MO, Lavergne O, Alby F, Cazales M, Baldin V, Thuriereau C, Harnett J, et al. (2004). A novel synthetic inhibitor of CDC25 phosphatases: BN82002. *Cancer Res* 64, 3320–3325. [PubMed: 15126376]
- Brezak MC, Valette A, Quaranta M, Contour-Galcera MO, Jullien D, Lavergne O, Frongia C, Bigg D, Kasprzyk PG, Prevost GP, and Ducommun B (2009). IRC-083864, a novel bis quinone inhibitor of CDC25 phosphatases active against human cancer cells. *Int. J. Cancer* 124, 1449–1456. [PubMed: 19065668]
- Busino L, Donzelli M, Chiesa M, Guardavaccaro D, Ganoh D, Dorrello NV, Hershko A, Pagano M, and Draetta GF (2003). Degradation of Cdc25A by beta-TrCP during S phase and in response to DNA damage. *Nature* 426, 87–91. [PubMed: 14603323]
- Caino MC, Ghosh JC, Chae YC, Vaira V, Rivadeneira DB, Favarsani A, Rampini P, Kossenkov AV, Aird KM, Zhang R, et al. (2015). PI3K therapy reprograms mitochondrial trafficking to fuel tumor cell invasion. *Proc. Natl. Acad. Sci. USA* 112, 8638–8643. [PubMed: 26124089]
- Cangi MG, Cukor B, Soung P, Signoretti S, Moreira G Jr., Ranashinge M, Cady B, Pagano M, and Loda M (2000). Role of the Cdc25A phosphatase in human breast cancer. *J. Clin. Invest* 106, 753–761. [PubMed: 10995786]
- Cho YC, Park JE, Park BC, Kim JH, Jeong DG, Park SG, and Cho S (2015). Cell cycle-dependent Cdc25C phosphatase determines cell survival by regulating apoptosis signal-regulating kinase 1. *Cell Death Differ* 22, 1605–1617. [PubMed: 25633196]
- Chou TC, and Talalay P (1984). Quantitative analysis of dose-effect relationships: the combined effects of multiple drugs or enzyme inhibitors. *Adv. Enzyme Regul* 22, 27–55. [PubMed: 6382953]
- Curtis C, Shah SP, Chin SF, Turashvili G, Rueda OM, Dunning MJ, Speed D, Lynch AG, Samarajiwa S, Yuan Y, et al. ; METABRIC Group (2012). The genomic and transcriptomic architecture of 2,000 breast tumours reveals novel subgroups. *Nature* 486, 346–352. [PubMed: 22522925]
- Dalvai M, Mondesert O, Bourdon JC, Ducommun B, and Dozier C (2011). Cdc25B is negatively regulated by p53 through Sp1 and NF-Y transcription factors. *Oncogene* 30, 2282–2288. [PubMed: 21242964]
- Davis ST, Benson BG, Bramson HN, Chapman DE, Dickerson SH, Dold KM, Eberwein DJ, Edelstein M, Frye SV, Gampe RT Jr., et al. (2002). Retraction. *Science* 298, 2327.
- Dominguez-Brauer C, Thu KL, Mason JM, Blaser H, Bray MR, and Mak TW (2015). Targeting mitosis in cancer: emerging strategies. *Mol. Cell* 60, 524–536. [PubMed: 26590712]
- Dvinge H, Git A, Gräf S, Salmon-Divon M, Curtis C, Sottoriva A, Zhao Y, Hirst M, Armisen J, Miska EA, et al. (2013). The shaping and functional consequences of the microRNA landscape in breast cancer. *Nature* 497, 378–382. [PubMed: 23644459]
- Finn RS, Dering J, Conklin D, Kalous O, Cohen DJ, Desai AJ, Ginther C, Atefi M, Chen I, Fowst C, et al. (2009). PD 0332991, a selective cyclin D kinase 4/6 inhibitor, preferentially inhibits proliferation of luminal estrogen receptor-positive human breast cancer cell lines in vitro. *Breast Cancer Res* 11, R77. [PubMed: 19874578]
- Galaktionov K, Chen X, and Beach D (1996). Cdc25 cell-cycle phosphatase as a target of c-myc. *Nature* 382, 511–517. [PubMed: 8700224]
- Gatza ML, Lucas JE, Barry WT, Kim JW, Wang Q, Crawford MD, Datto MB, Kelley M, Mathey-Prevot B, Potti A, et al. (2010). A pathway-based classification of human breast cancer. *Proc. Natl. Acad. Sci. U S A* 107, 6994–6999. [PubMed: 20335537]
- Goel S, DeCristo MJ, Watt AC, BrinJones H, Sceneay J, Li BB, Khan N, Ubellacker JM, Xie S, Metzger-Filho O, et al. (2017). CDK4/6 inhibition triggers anti-tumour immunity. *Nature* 548, 471–475. [PubMed: 28813415]

- Guo J, Parise RA, Joseph E, Lan J, Pan SS, Joo B, Egorin MJ, Wipf P, Lazo JS, and Eiseman JL (2007). Pharmacology and antitumor activity of a quinolinedione Cdc25 phosphatase inhibitor DA3003-1 (NSC 663284). *Anticancer Res* 27 (5A), 3067–3073. [PubMed: 17970046]
- Guo SL, Ye H, Teng Y, Wang YL, Yang G, Li XB, Zhang C, Yang X, Yang ZZ, and Yang X (2013). Akt-p53-miR-365-cyclin D1/cdc25A axis contributes to gastric tumorigenesis induced by PTEN deficiency. *Nat. Commun* 4, 2544. [PubMed: 24149576]
- Hazzalin CA, Le Panse R, Cano E, and Mahadevan LC (1998). Anisomycin selectively desensitizes signalling components involved in stress kinase activation and fos and jun induction. *Mol. Cell. Biol* 18, 1844–1854. [PubMed: 9528756]
- He R, Zeng LF, He Y, Zhang S, and Zhang ZY (2013). Small molecule tools for functional interrogation of protein tyrosine phosphatases. *FEBS J* 280, 731–750. [PubMed: 22816879]
- Herrera-Abreu MT, Palafox M, Asghar U, Rivas MA, Cutts RJ, Garcia-Murillas I, Pearson A, Guzman M, Rodriguez O, Grueso J, et al. (2016). Early adaptation and acquired resistance to CDK4/6 inhibition in estrogen receptor-positive breast cancer. *Cancer Res* 76, 2301–2313. [PubMed: 27020857]
- Herschkowitz JI, Simin K, Weigman VJ, Mikaelian I, Usary J, Hu Z, Rasmussen KE, Jones LP, Assefnia S, Chandrasekharan S, et al. (2007). Identification of conserved gene expression features between murine mammary carcinoma models and human breast tumors. *Genome Biol* 8, R76. [PubMed: 17493263]
- Herschkowitz JI, He X, Fan C, and Perou CM (2008). The functional loss of the retinoblastoma tumour suppressor is a common event in basal-like and luminal B breast carcinomas. *Breast Cancer Res* 10, R75. [PubMed: 18782450]
- Jiang Z, Deng T, Jones R, Li H, Herschkowitz JI, Liu JC, Weigman VJ, Tsao MS, Lane TF, Perou CM, and Zacksenhaus E (2010). Rb deletion in mouse mammary progenitors induces luminal-B or basal-like/EMT tumor subtypes depending on p53 status. *J. Clin. Invest* 120, 3296–3309. [PubMed: 20679727]
- Jiang Z, Jones R, Liu JC, Deng T, Robinson T, Chung PE, Wang S, Herschkowitz JI, Egan SE, Perou CM, and Zacksenhaus E (2011). RB1 and p53 at the crossroad of EMT and triple-negative breast cancer. *Cell Cycle* 10, 1563–1570. [PubMed: 21502814]
- Jones RA, Robinson TJ, Liu JC, Shrestha M, Voisin V, Ju Y, Chung PE, Pellicchia G, Fell VL, Bae S, et al. (2016). RB1 deficiency in triple-negative breast cancer induces mitochondrial protein translation. *J. Clin. Invest* 126, 3739–3757. [PubMed: 27571409]
- Kitajima S, and Takahashi C (2017). Intersection of retinoblastoma tumor suppressor function, stem cells, metabolism, and inflammation. *Cancer Sci* 108, 1726–1731. [PubMed: 28865172]
- Knudsen ES, and Witkiewicz AK (2017). The strange case of CDK4/6 inhibitors: mechanisms, resistance, and combination strategies. *Trends Cancer* 3, 39–55. [PubMed: 28303264]
- Koboldt DC, Fulton RS, McLellan MD, Schmidt H, Kalicki-Veizer J, McMichael JF, Fulton LL, Dooling DJ, Ding L, Mardis ER, et al. : Cancer Genome Atlas Network (2012). Comprehensive molecular portraits of human breast tumours. *Nature* 490, 61–70. [PubMed: 23000897]
- Kristjánisdóttir K, and Rudolph J (2004). Cdc25 phosphatases and cancer. *Chem. Biol* 11, 1043–1051. [PubMed: 15324805]
- Kuntz EM, Baquero P, Michie AM, Dunn K, Tardito S, Holyoake TL, Helgason GV, and Gottlieb E (2017). Targeting mitochondrial oxidative phosphorylation eradicates therapy-resistant chronic myeloid leukemia stem cells. *Nat. Med* 23, 1234–1240. [PubMed: 28920959]
- Lawrence RT, Perez EM, Hernández D, Miller CP, Haas KM, Irie HY, Lee SI, Blau CA, and Villén J (2015). The proteomic landscape of triple-negative breast cancer. *Cell Rep* 11, 630–644. [PubMed: 25892236]
- Liu H, Nishitoh H, Ichijo H, and Kyriakis JM (2000). Activation of apoptosis signal-regulating kinase 1 (ASK1) by tumor necrosis factor receptor-associated factor 2 requires prior dissociation of the ASK1 inhibitor thioredoxin. *Mol. Cell. Biol* 20, 2198–2208. [PubMed: 10688666]
- Liu TJ, Koul D, LaFortune T, Tiao N, Shen RJ, Maira SM, Garcia-Echeverria C, and Yung WK (2009). NVP-BEZ235, a novel dual phosphatidylinositol 3-kinase/mammalian target of rapamycin inhibitor, elicits multifaceted antitumor activities in human gliomas. *Mol. Cancer Ther* 8, 2204–2210. [PubMed: 19671762]

- Liu JC, Voisin V, Wang S, Wang DY, Jones RA, Datti A, Uehling D, Al-awar R, Egan SE, Bader GD, et al. (2014). Combined deletion of Pten and p53 in mammary epithelium accelerates triple-negative breast cancer with dependency on eEF2K. *EMBO Mol. Med* 6, 1542–1560. [PubMed: 25330770]
- Liu H, Tang X, Srivastava A, Pécot T, Daniel P, Hemmelgarn B, Reyes S, Fackler N, Bajwa A, Kladney R, et al. (2015). Redeployment of Myc and E2f1–3 drives Rb-deficient cell cycles. *Nat. Cell Biol* 17, 1036–1048. [PubMed: 26192440]
- Ma CX, Janetka JW, and Piwnica-Worms H (2011). Death by releasing the breaks: CHK1 inhibitors as cancer therapeutics. *Trends Mol. Med.* 17, 88–96. [PubMed: 21087899]
- Medema RH, and Macrek L (2012). Checkpoint control and cancer. *Oncogene* 31, 2601–2613. [PubMed: 21963855]
- Nik-Zainal S, Davies H, Staaf J, Ramakrishna M, Glodzik D, Zou X, Martincorena I, Alexandrov LB, Martin S, Wedge DC, et al. (2016). Landscape of somatic mutations in 560 breast cancer whole-genome sequences. *Nature* 534, 47–54. [PubMed: 27135926]
- Otto T, and Sicinski P (2017). Cell cycle proteins as promising targets in cancer therapy. *Nat. Rev. Cancer* 17, 93–115. [PubMed: 28127048]
- Prat A, and Perou CM (2011). Deconstructing the molecular portraits of breast cancer. *Mol. Oncol* 5, 5–23. [PubMed: 21147047]
- Prat A, Parker JS, Karginova O, Fan C, Livasy C, Herschkowitz JI, He X, and Perou CM (2010). Phenotypic and molecular characterization of the claudin-low intrinsic subtype of breast cancer. *Breast Cancer Res* 12, R68. [PubMed: 20813035]
- Robinson TJ, Liu JC, Vizeacoumar F, Sun T, Maclean N, Egan SE, Schimmer AD, Datti A, and Zacksenhaus E (2013). RB1 status in triple negative breast cancer cells dictates response to radiation treatment and selective therapeutic drugs. *PLoS ONE* 8, e78641. [PubMed: 24265703]
- Robinson DR, Wu YM, Lonigro RJ, Vats P, Cobain E, Everett J, Cao X, Rabban E, Kumar-Sinha C, Raymond V, et al. (2017). Integrative clinical genomics of metastatic cancer. *Nature* 548, 297–303. [PubMed: 28783718]
- Santamaría D, Barrière C, Cerqueira A, Hunt S, Tardy C, Newton K, Cáceres JF, Dubus P, Malumbres M, and Barbacid M (2007). Cdk1 is sufficient to drive the mammalian cell cycle. *Nature* 448, 811–815. [PubMed: 17700700]
- Tibbles LA, and Woodgett JR (1999). The stress-activated protein kinase pathways. *Cell. Mol. Life Sci* 55, 1230–1254. [PubMed: 10487205]
- Tyanova S, Albrechtsen R, Kronqvist P, Cox J, Mann M, and Geiger T (2016). Proteomic maps of breast cancer subtypes. *Nat. Commun* 7, 10259. [PubMed: 26725330]
- Vigo E, Müller H, Prosperini E, Hateboer G, Cartwright P, Moroni MC, and Helin K (1999). CDC25A phosphatase is a target of E2F and is required for efficient E2F-induced S phase. *Mol. Cell. Biol* 19, 6379–6395. [PubMed: 10454584]
- Viré E, Curtis C, Davalos V, Git A, Robson S, Villanueva A, Vidal A, Barbieri I, Aparicio S, Esteller M, et al. (2014). The breast cancer oncogene EMSY represses transcription of antimetastatic microRNA miR-31. *Mol. Cell* 53, 806–818. [PubMed: 24582497]
- Wang S, Liu JC, Kim D, Datti A, and Zacksenhaus E (2016). Targeted Pten deletion plus p53-R270H mutation in mouse mammary epithelium induces aggressive claudin-low and basal-like breast cancer. *Breast Cancer Res* 18, 9. [PubMed: 26781438]
- Wang S, Liu JC, Ju Y, Pellicchia G, Voisin V, Wang DY, Leha LR, Ben-David Y, Bader GD, and Zacksenhaus E (2017). microRNA-143/145 loss induces Ras signaling to promote aggressive Pten-deficient basal-like breast cancer. *JCI Insight* 2, 93313. [PubMed: 28768903]
- Witkiewicz AK, Chung S, Brough R, Vail P, Franco J, Lord CJ, and Knudsen ES (2018). Targeting the vulnerability of RB tumor suppressor loss in triple-negative breast cancer. *Cell Rep* 22, 1185–1199. [PubMed: 29386107]
- Zacksenhaus E, Shrestha M, Liu JC, Vorobieva I, Chung PED, Ju Y, Nir U, and Jiang Z (2017). Mitochondrial OXPHOS induced by RB1 deficiency in breast cancer: implications for anabolic metabolism, stemness, and metastasis. *Trends Cancer* 3, 768–779. [PubMed: 29120753]

Zou X, Tsutsui T, Ray D, Blomquist JF, Ichijo H, Ucker DS, and Kiyokawa H (2001). The cell cycle-regulatory CDC25A phosphatase inhibits apoptosis signal-regulating kinase 1. *Mol. Cell. Biol* 21, 4818–4828. [PubMed: 11416155]

Author Manuscript

Author Manuscript

Author Manuscript

Author Manuscript

Highlights

- CDC25 inhibitors target TNBCs that are refractory to CDK4/6 plus CDK2 inhibition
- CDC25 mRNA levels are affected by RB1, PTEN, TP53, and MYC status in TNBC
- CDC25 plus WEE1 or PI3K inhibitors synergize to effectively suppress growth of TNBCs
- Provides a rational for development of CDC25-based therapy for TNBC

(C) GSEA visualized by Enrichment Map in Cytoscape showing most significant pathways enriched in *Rb/p53* (red) versus *Pten/p53* (blue) tumors. Green lines indicate connections of overlapping pathways. A complete GSEA profile is shown in Figure S2A.

(D) Heatmap showing the expression of genes on the CDC25 pathway in indicated mouse models. Expression of *Cdc25B* and *Cdc25C* is significantly higher in *p53*, *Rb/p53*, and *Pten/p53* relative to *Pten* tumors or normal mammary glands, respectively (statistical analysis is given in Figure S3).

See also Figures S2 and S3.

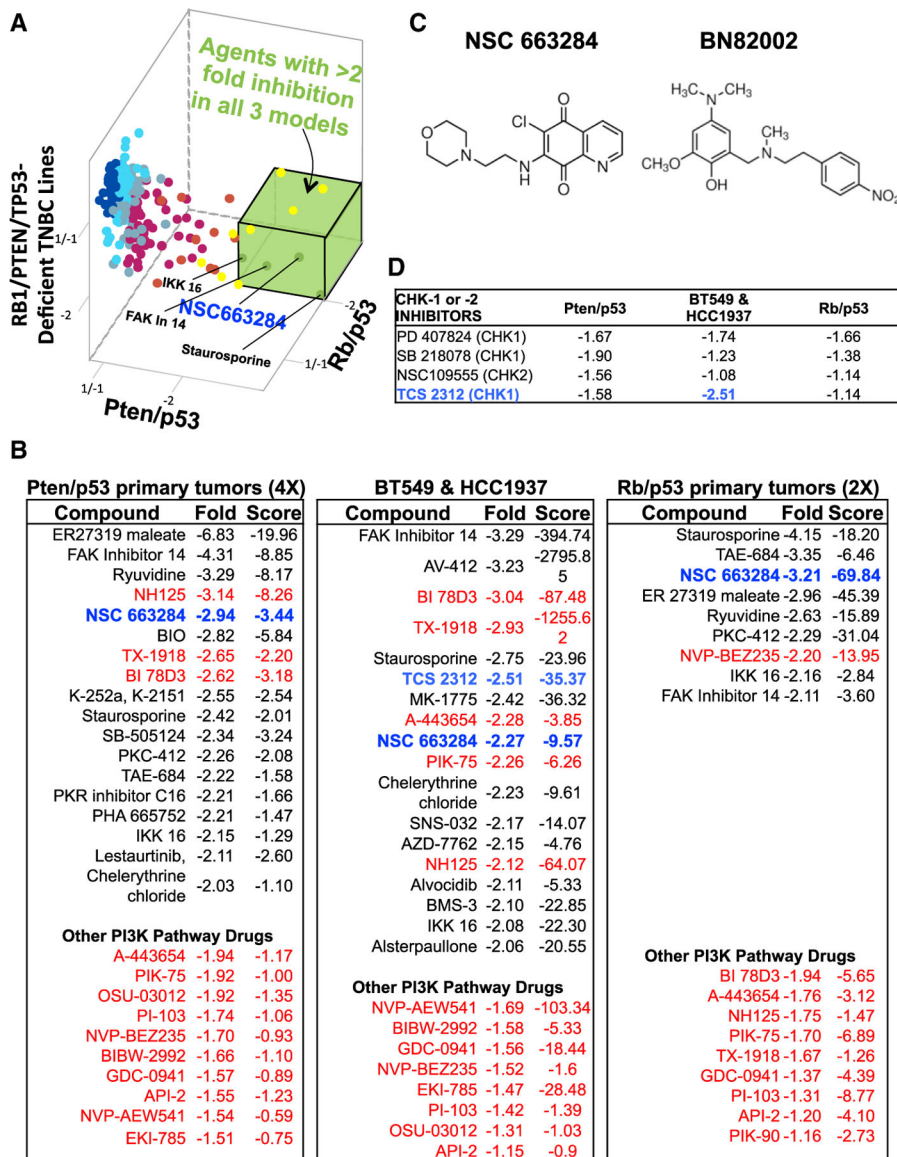


Figure 2. Identification of *RBI/PTEN/TP53*-Deficient TNBC-Suppressing Compounds

(A) 3D representation (fold change calculated compared to non-treated cells) of kinase/phosphatase inhibitor screens on primary mouse *Pten/p53* tumor, mouse *Rb/p53* primary tumor cells, and human *RBI/PTEN/TP53*-deficient TNBC cell lines (BT549 and HCC1937). Compounds with >2-fold inhibition on all three models of TNBC cells (green box) are indicated.

(B) Top inhibitory compounds with fold change and T score (difference divided by SD) for the three groups of tumor cells. The CDC25 inhibitor NSC663284 is highlighted in blue; CHK1 inhibitor TCS-2312 is indicated in light blue; PI3K pathway inhibitors are indicated in red.

(C) Chemical structure of CDC25 inhibitors NSC663284 and BN82002.

(D) Effects of CHK1 and CHK2 inhibitors with fold change on the three groups of tumor cells.

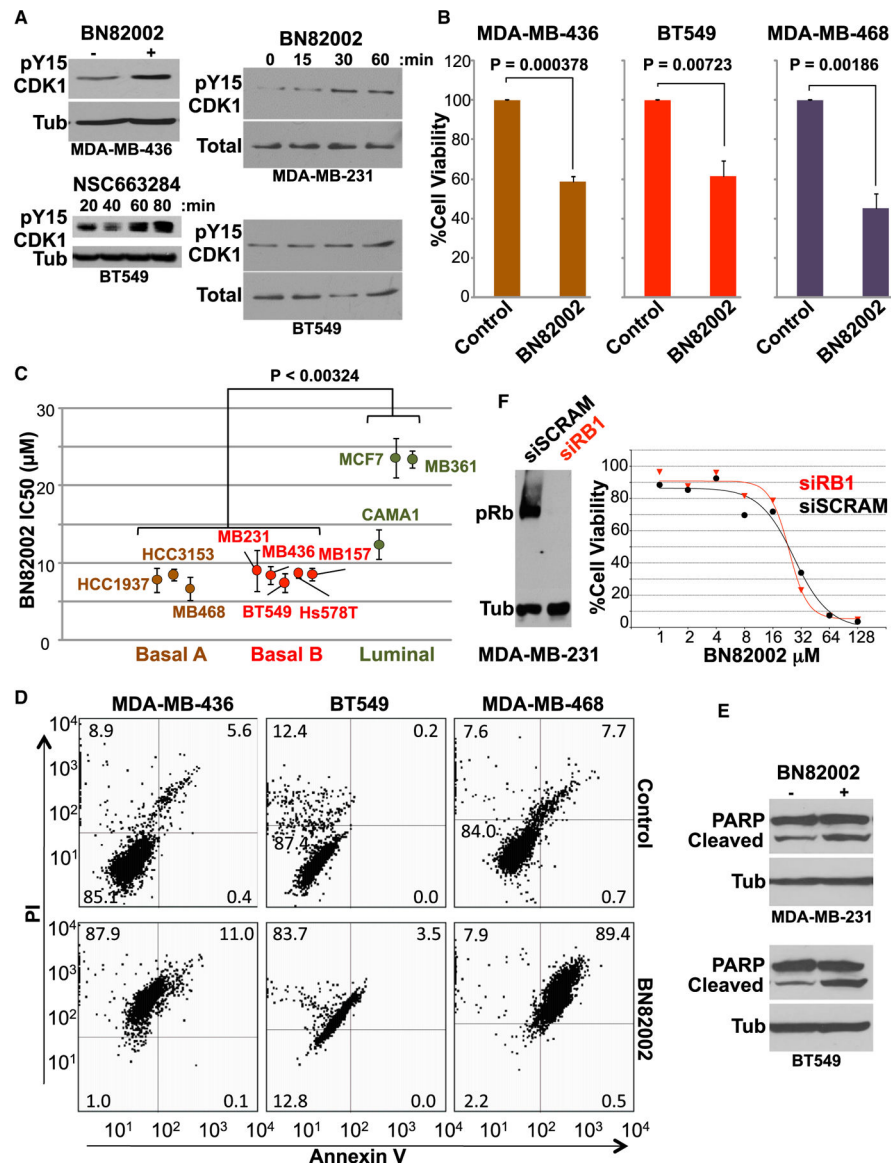


Figure 3. RB1-Deficient TNBC Cells Are Sensitive to CDC25 Inhibition

(A) Induction of CDK1 Tyr15 phosphorylation by the CDC25 inhibitors BN82002 and NSC663284. Indicated human TNBC cells were treated with inhibitors for 60 min or indicated time periods and were immunoblotted with anti-pY15 CDK1 antibody. Antibodies for tubulin or total CDK1 served as loading controls.

(B) Significant inhibition of RB1-deficient TNBC (BT549, MDA-MB-436, and MDA-MB-468) cell proliferation by BN82002 (10 μ M). Average and SD were calculated from 5 independent experiments.

(C) IC₅₀ \pm SD of BN82002 in indicated luminal (CAMA1, MCF7, and MDA-MB-361), basal A (basal-like; HCC3153, MDA-MB-468, and HCC1937), and basal B (claudin-low; BT549, Hs578T, MDA-MB-157, MDA-MB-231, and MDA-MB-436) BC lines. The p value denotes one-way ANOVA with Tukey post hoc.

(D) Induction of apoptosis by CDC25 inhibitors in TNBC cells. Levels of apoptosis were determined by flow cytometry of annexin V- and PI-stained TNBC cells (BT549, MDA-MB-436, and MDA-MB-468) after BN82002 (10 μ M) treatment.

(E) Induction of PARP cleavage 24 hr post-CDC25 inhibition in indicated TNBC cells.

(F) Left: efficient *RBI* knockdown in MDA-MB-231 cells. Cells were transfected with *RBI*-specific or scrambled RNAi and analyzed for pRb expression 3 days later. Right: knockdown of *RBI* via RNAi does not reduce sensitivity of MDA-MB-231 cells to BN82002.

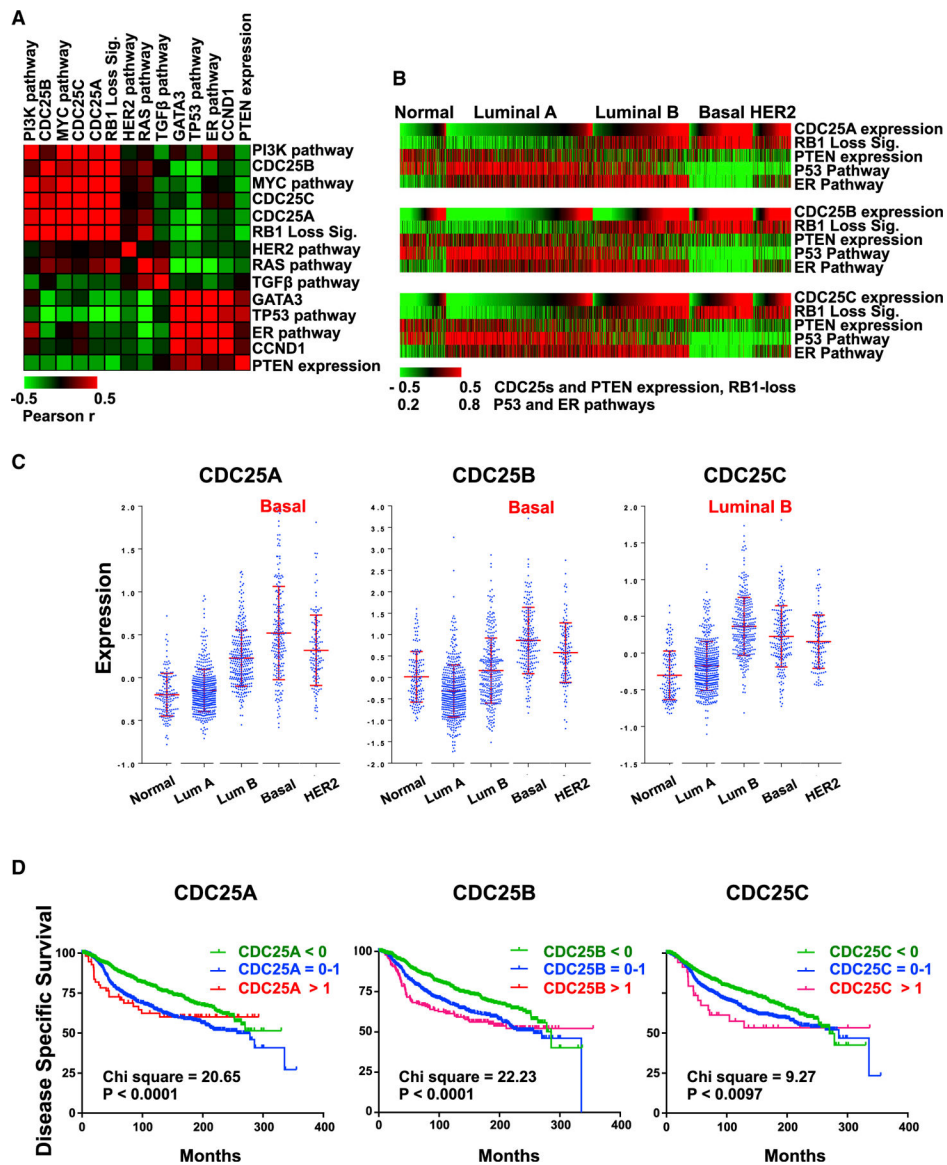


Figure 4. Expression of *CDC25* Genes in Different BC Subtypes, Correlation with Various Oncogenic Alterations, and Impact on Clinical Outcome in Breast Cancer

(A) Pairwise correlation analysis comparing *CDC25* expression with indicated levels of oncogenes and tumor suppressors estimated by signatures, pathway activities, or gene expression in 1,302 BC samples using European Genome-phenome Archive: EGAD0010000434 (EGA; <http://www.ebi.ac.uk/ega/>). Results are organized by hierarchical clustering using Pearson correlations. Heatmap indicates the correlation coefficient values: red indicates positive correlation, and green indicates negative correlation.

(B) Correlation of *CDC25* expression and tumor suppressor gene status in each BC subtype. The 1,302 BCs grouped by subtypes were ordered with *CDC25A*, *CDC25B*, and *CDC25C* expression values from low to high in each subtype. In all subtypes, expression of the three *CDC25* genes correlates with loss of RB1, PTEN, TP53, and ER (positively with *RB1* loss; negatively with *PTEN* expression, TP53, and ER pathway activity). For statistical analysis, see Figure S4.

(C) Expression distribution of *CDC25A*, *CDC25B*, and *CDC25C* in different BC subtypes. Highest expression of *CDC25A* and *CDC25B* was in basal-like BC; highest *CDC25C* expression was in luminal B. Error bars indicate mean \pm SD; $p < 0.0001$ by ANOVA.

(D) Kaplan-Meier analysis of the 1,302 BC patients in correlation with *CDC25A*, *CDC25B*, and *CDC25C* expression; low, <0 ; medium, $0-1$; high, >1 . Indicated chi-square and p values were calculated using log-rank (Mantel-Cox) analysis.

See also Figure S4.

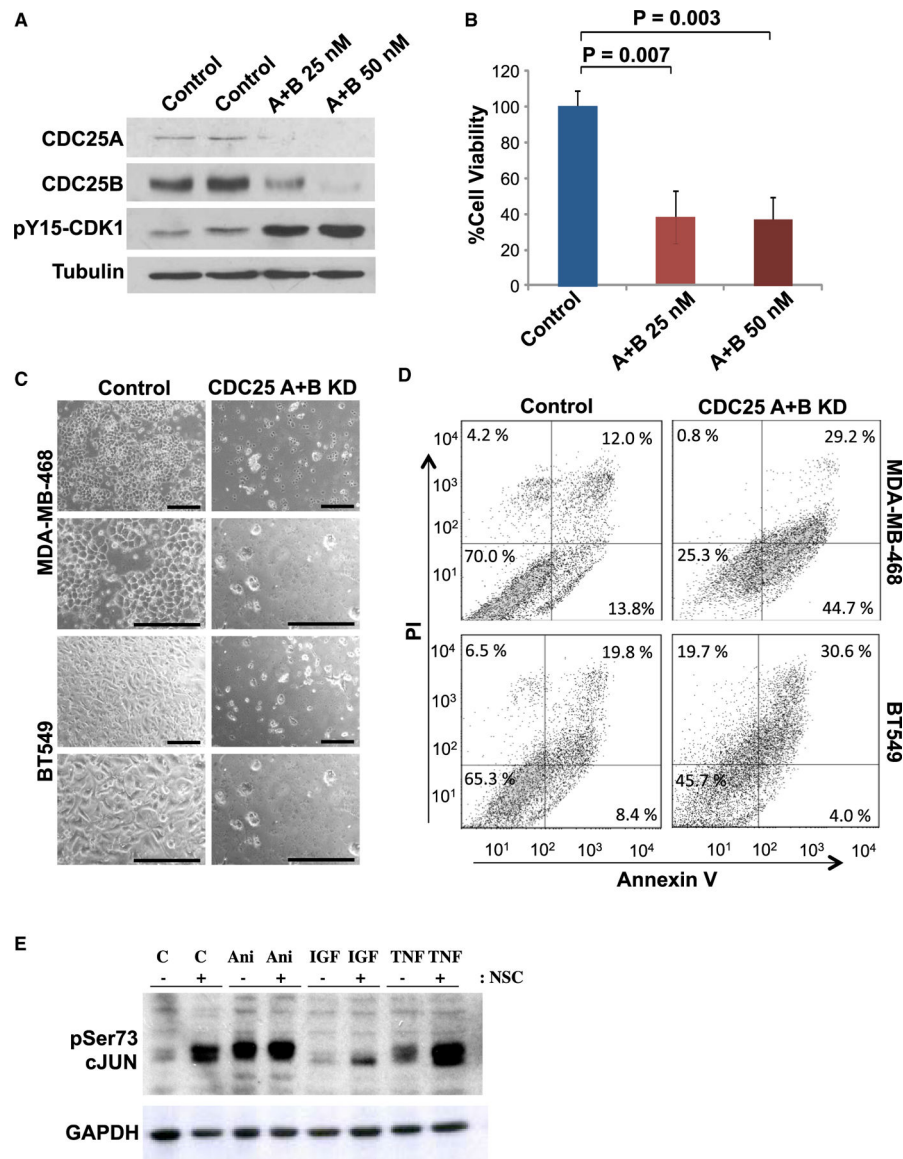


Figure 5. Knockdown of *CDC25A* Plus *CDC25B* Suppresses Growth of *RB1*-Deficient TNBC Cells *In Vitro*

(A) BT549 cells were transfected with scrambled RNAi control or *CDC25A* plus *CDC25B* RNAi, at concentrations of 25 or 50 nM, and 3 days later were analyzed for *CDC25A*, *CDC25B*, and p-CDK1 expression by immunoblotting. Tubulin served as loading control.

(B) BT549 cells transfected as described above were analyzed for growth by MTT assay. Error bars indicate SD; p values calculated by 2 tailed Student's t test.

(C) Representative images of MDA-MB-468 and BT549 cells following double transfection with 25 nM control or *CDC25A* plus *CDC25B* RNAi. Scale bars, 20 μ M.

(D) Representative flow cytometry analysis of annexin V/PI-stained MDA-MB-468 and BT549 cells co-transfected with *CDC25A* and *CDC25B* RNAi at a concentration of 25 nM each.

(E) Induction of Ser73-cJUN phosphorylation 24 hr post-treatment with *CDC25* inhibitors. MDA-MB-231 cells were treated with DMSO or 4 μ M NSC663284 for 24 hr and then were

exposed to anisomycin (Ani; 3 $\mu\text{g}/\text{mL}$) for 30 min or to IGF1 (IGF; 50 ng/mL) or TNF- α (TNF; 100 ng/mL) for 15 min and immunoblotted for Ser73-c-JUN. GAPDH served as loading control.

Author Manuscript

Author Manuscript

Author Manuscript

Author Manuscript

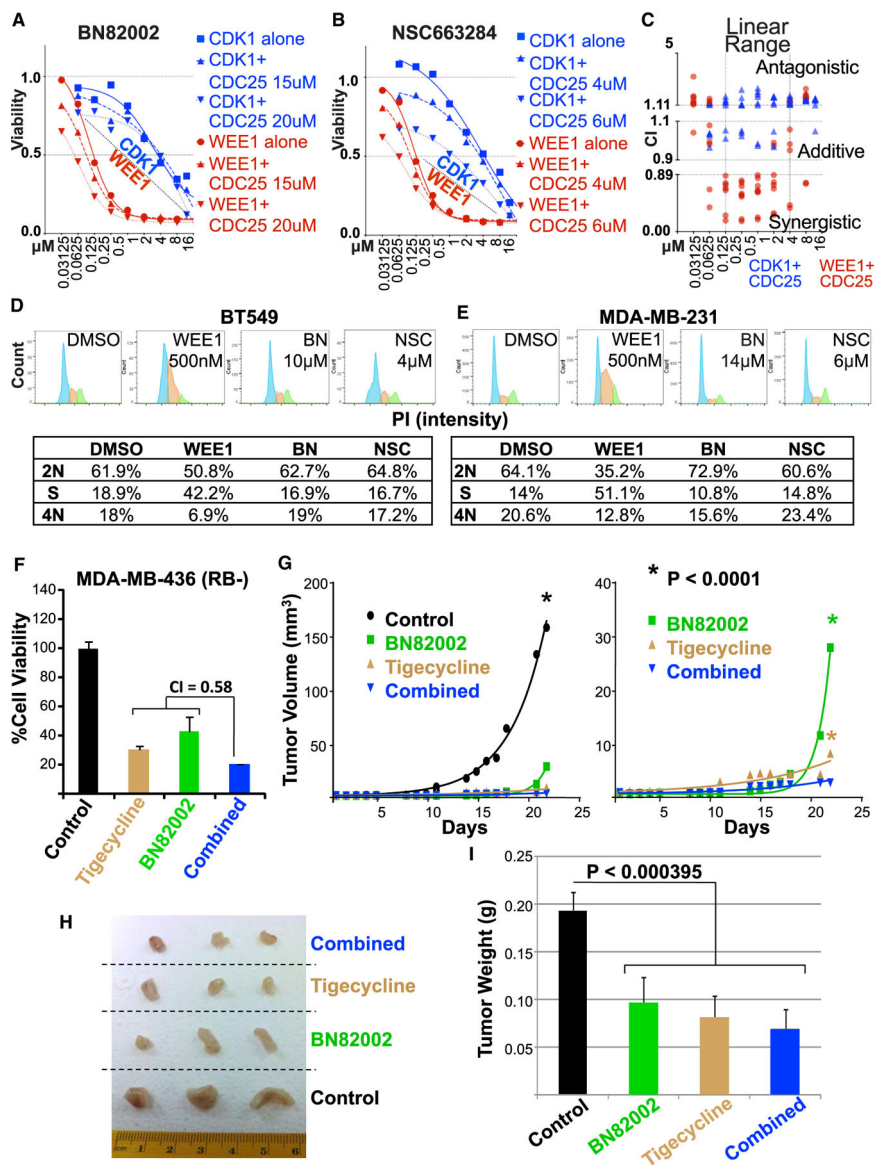


Figure 6. Synergy Between CDC25 Inhibitors and a WEE1 Inhibitor *In Vitro* and with the Mitochondrial Protein Translation Inhibitor, Tigecycline, *In Vivo*
 (A and B) Combined CDC25 inhibitors (A) BN82002 or (B) NSC663284 plus CDK1 inhibitor (RO3306) show additive/antagonistic effects, whereas CDC25 plus the WEE1 inhibitor (MK-1775) are mostly synergistic in BT549 TNBC cells. Similar results obtained with MDA-MB-231 cells are shown in Figures S7B and S7C.
 (C) Combination index calculated by CompuSyn software for the two CDC25 inhibitors plus CDK1 (blue) or the WEE1 (red) inhibitors in BT549 and MDA-MB-231. See Figure S7D for details of each inhibitor and cell line.

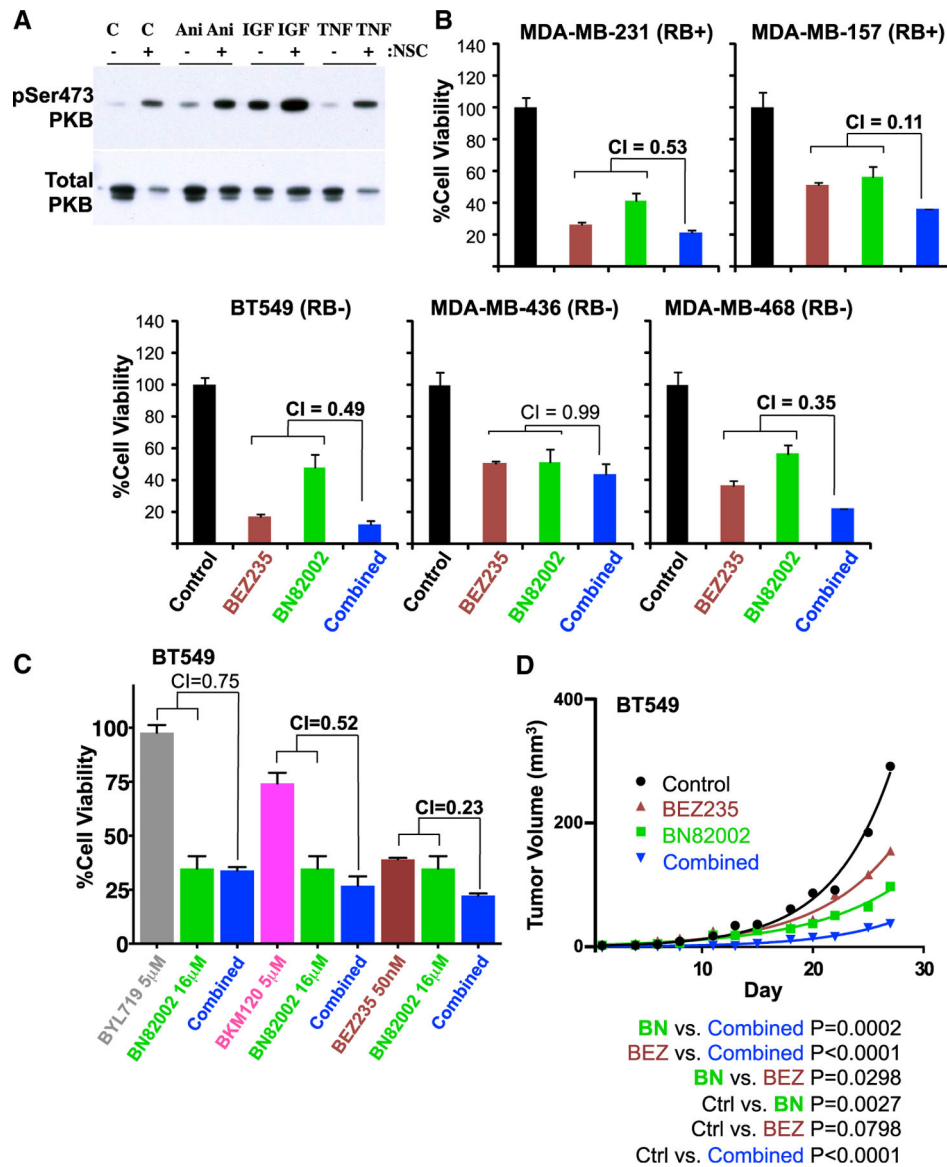


Figure 7. CDC25 Inhibition Synergizes with PI3K Inhibitors to Suppress Diverse TNBCs

(A) Induction of Ser473-PKB/AKT phosphorylation 24 hr post-CDC25 inhibition. MDA-MB-231 cells were treated with DMSO or 4 μM NSC663284 for 24 hr and then exposed to anisomycin (Ani; 3 μg/mL) for 30 min, and to IGF1 (IGF; 50 ng/mL) or TNF-α (TNF; 100 ng/mL) for 15 min, and immunoblotted with phospho-Ser473-PKB/AKT. Total PKB/AKT is shown below.

(B) Response of indicated TNBC cell lines to BN82002 (10 μM) alone or in combination with BEZ235 (Dactolisib; 0.3 μM). Synergy between the two compounds was assessed by combination index (CI) using Compusyn software.

(C) Cell viability of BT549 cells treated with the CDC25 inhibitor, BN82002, and 3 different PI3K inhibitors: BYL719, BMK120, or BEZ235.

(D) Effect of the CDC25 inhibitor, BN82002, and the PI3K/mTOR inhibitor BEZ235 on TNBC xenograft growth. NSG mice were injected in the inguinal fat pad with BT549 cells

(1×10^6) in Matrigel. Once palpable tumors formed, mice were injected i.p. 3 times per week for 27 days with DMSO or with 15 mg/kg BN82002, 5 mg/kg BEZ235, or both. Tumors were measured on each day of treatment. Control, n = 4; BN82002, n = 4; BEZ235, n = 4; and BN82002 and BEZ235 combined, n = 3 mice. Differences between groups (p value) were calculated by nonlinear regression using GraphPad PRISM 6.

(D and E) Cell-cycle profiles of (D) BT549 (RB1⁻) and (E) MDA-MB-231 (RB1⁺) cells treated with DMSO (vehicle control) or indicated concentrations of WEE1 inhibitor (MK-1775) or CDC25 inhibitors (BN82002 or NSC663284) using PI staining and flow cytometry analysis. The percentage of cells in each phase is indicated, excluding cells with <2N or >4N DNA.

(F) Response of RB1⁻ TNBC MDA-MB-436 cells to treatment with BN82002 (10 μ M) alone or in combination with tigecycline (10 μ M). Error bars indicate SD. Level of synergy between the two compounds was assessed by combination index (CI), using CompuSyn software. A similar analysis of BT549 and MDA-MB-468 cells showing lack of synergy is depicted in Figure S8.

(G) Left: drug-response curves for RB1-deficient MDA-MB-436 tumor xenografts untreated or treated with BN82002 and/or tigecycline. Tumor cells were injected orthotopically, and once palpable tumors were formed, mice (n = 6 per group) were injected 3 times per week for 21 days with DMSO (vehicle) or with 15 mg/kg BN82002, 50 mg/kg tigecycline or both. Right: the control graph for the untreated mice was removed to better highlight differences between the treated groups.

*p < 0.0001, by non-linear regression (GraphPad Prism 5.0).

(H) Appearance of 3 representative tumors of each group from (G).

(I) Significant reduction of final tumor weight in treatment groups compared to control. Error bars indicate SD. The p value was calculated by ANOVA.

See also Figures S7 and S8.